Nishi *et al.*
Progress in Earth and Planetary Science (2023) 10:41
https://doi.org/10.1186/s40645-023-00572-0

Progress in Earth and Planetary Science

RESEARCH ARTICLE

Open Access

Effect of grain size on amorphization mechanism and kinetics of bridgmanite in shocked meteorites

Masayuki Nishi[1*], Si Jin[1], Katsutoshi Kawano[1], Hideharu Kuwahara[2], Akihiro Yamada[3,4], Shogo Kawaguchi[5], Yuki Mori[5], Tatsuhiro Sakaiya[1] and Tadashi Kondo[1]

Abstract

Bridgmanite formation and amorphization in shocked meteorites constrain the pressure and temperature conditions during planetary impact. However, the effect of the bridgmanite grain size on its amorphization kinetics is still unclear. Here, the amorphization mechanism and kinetics of fine-grained polycrystalline bridgmanite were studied at high temperatures up to 1080 K. High-temperature time-resolved synchrotron X-ray diffraction measurements showed that significant volume expansion due to temperature-induced amorphization caused static stress, which then hindered amorphization progress. Further, the temperature required for the amorphization of fine-grained bridgmanite (~ 1 μm) was found to be approximately 100 K higher than that required for the amorphization of coarse-grained samples (> 10 μm). We also noted that amorphization preferentially commenced at the twin planes and subgrain boundaries of bridgmanite grains, resulting in lower amorphization temperatures for the coarse-grained samples. The limited number of such specific locations in fine-grained natural bridgmanite suggested that grain boundary amorphization may be the dominant mechanism for bridgmanite amorphization in shocked meteorites. This unique amorphization kinetics would support the preservation of bridgmanite during the post-shock annealing in the shocked meteorite. Although bridgmanite amorphization starts easily at temperatures above ~ 420 K, a small amount of bridgmanite grains can survive at temperatures above 800 K by the effect of amorphization-induced stress.

Keywords Bridgmanite, High pressure, Shocked meteorite, Amorphization kinetics

1 Introduction

High-pressure and high-temperature generation induced by planetary impact processes can cause constituent minerals to undergo phase transitions, forming their high-pressure polymorphs (Gillet and El Goresy 2013; Hu and Sharp 2022; Stöffler et al. 2018). Further, high-pressure minerals, such as stishovite, majorite, ringwoodite, and bridgmanite, can be found in shocked meteorites that have fallen on Earth (Binns et al. 1969; El Goresy et al. 2004; Ohtani et al. 2011; Smith and Mason 1970; Tomioka and Miyahara 2017; Tschauner et al. 2014). These high-pressure minerals can be formed within a few seconds, corresponding to the timescale of shock-induced high-pressure pulses during impact (Beck et al. 2005; Gillet and El Goresy 2013;

*Correspondence:
Masayuki Nishi
nishimasa@ess.sci.osaka-u.ac.jp
[1] Department of Earth and Space Science, Osaka University, 1-1 Machikaneyama-cho, Toyonaka, Osaka 560-0043, Japan
[2] Geodynamics Research Center, Ehime University, 2-5 Bunkyo-cho, Matsuyama, Ehime 790-8577, Japan
[3] Department of Material Science, The University of Shiga Prefecture, Hikone, Shiga, Japan
[4] Center for Glass Science and Technology, The University of Shiga Prefecture, 2500, Hassaka-cho, Hikone, Shiga 522-8533, Japan
[5] Japan Synchrotron Radiation Research Institute, Sayo-gun, Hyogo 679-5198, Japan

Ohtani et al. 2004; Tiwari et al. 2022). However, they become metastable immediately after pressure release. Since the high temperature after pressure release (hereafter, residual post-shock temperature) is maintained over several hours, high-pressure minerals often disappear owing to back transformation or amorphization (Hu and Sharp 2017; Kimura et al. 2004). Reportedly, the kinetics of these reactions strongly depend on temperature, and possibly, the residual post-shock temperature is a key parameter that determines whether high-pressure minerals can survive in shocked meteorites (Kubo et al. 2022; Nishi et al. 2022).

The occurrence of bridgmanites in shocked meteorites (Ghosh et al. 2021; Miyahara et al. 2011; Tiwari et al. 2021; Tomioka and Fujino 1997; Tschauner et al. 2014) suggests that pressures above 23 GPa are generated during the impact process. Additionally, the residual post-shock temperature should be sufficiently low to preserve the structure of bridgmanite, which is known to be easily destroyed at high temperatures above 400 K and atmospheric pressure (Durben and Wolf 1992; Wang et al. 1992). At much higher temperatures above ~ 800 K, bridgmanite transforms to enstatite (Knittle and Jeanloz 1987). A recent experimental study based on time-resolved in situ X-ray diffraction (XRD) measurements showed that the amorphization of polycrystalline bridgmanite with grain size > 10 μm starts at temperatures above ~ 400 K and ends at ~ 700 K, irrespective of the annealing time (Nishi et al. 2022). It has also been observed that amorphization progress at a constant temperature is strongly prevented by static stress, which is induced by volume expansion via amorphization. This stress effect enables the preservation of bridgmanite during exposure to the residual post-shock temperature, which continues for several hours. Additionally, based on microtextural observations, it has been inferred that intracrystalline amorphization is initiated at specific weak locations within bridgmanite grains, such as twin planes and subgrain boundaries. However, the grain size corresponding to natural samples is below ~ 1 μm and conspicuous dislocations are absent in small grains (Ghosh et al. 2021; Tomioka and Fujino 1997; Tschauner et al. 2014). Therefore, intracrystalline amorphization may not be the dominant mechanism of the amorphization of natural bridgmanite.

Here, we subjected bridgmanite to time-resolved in situ XRD measurements during amorphization to clarify the effect of grain size on bridgmanite amorphization at high temperatures. To this end, we used bridgmanite with a grain size one order of magnitude smaller than that used in a previous study (Nishi et al. 2022).

2 Methods

Polycrystalline bridgmanite was synthesized from $MgSiO_3$ glass at 25 GPa and 1400 °C using a 3000-ton multi-anvil apparatus (Orange-3000) at the Geodynamics Research Center, Ehime University, Japan. First, $MgSiO_3$ glass was synthesized from a mixture of reagent-grade MgO and SiO_2 via melting in a high-temperature furnace. The recovered bulk glass was then shaped into a rod (diameter = 2.5 mm) using an ultrasonic machining tool. To avoid moisture adsorption, which causes rapid grain growth, we used bulk glass without crushing. The cell assembly and anvils were almost the same as that used in our previous study (Nishi et al. 2022).

Time-resolved high-temperature XRD measurements on the polycrystalline bridgmanite were performed at beamline BL02B2, SPring-8, Japan (Kawaguchi et al. 2017). Specifically, the synthesized polycrystalline bridgmanite was crushed into several pieces and filled in silica glass capillaries (diameter = 0.5 mm). The incident X-ray beam, size 1.5 × 0.5 mm, larger than that of the polycrystalline sample, was monochromatized to 25 keV using Si(111) double crystals. The wavelength was determined to be 0.496431 Å using a standard reference material, CeO_2. XRD patterns were then obtained every 10 s during heating. The fluctuation of incident X-ray intensity monitored during the measurements was within 0.1%. The temperature was controlled using an N_2 gas blower. In runs FBRD07-09, the temperature was raised to the target value at a heating rate of 80 K/min and maintained for 2–30 min to observe the amorphization kinetics at a constant temperature (Table 1). The heating rates employed in the other runs were controlled at 10–30 K/min, and changes in peak intensity and bridgmanite lattice volume as a function of temperature were noted. The integrated intensities of the XRD and cell volumes of the crystals during heating were calculated using diffraction lines 020, 112, 200, 210, 211, 022, 122, 221, and 204 relative to the initial intensities before heating. Secondary electron images, obtained using a field-emission scanning electron microscope (JSM-IT500HR), were used to observe the texture of the recovered bridgmanite.

3 Results

We synthesized fine-grained polycrystalline bridgmanite with grain size (G) ~ 0.9 μm (Fig. 1a), much smaller than that of bridgmanite synthesized in a previous study (Nishi et al. 2022). G was estimated from the relationship: $G = cL$, where c is a constant with a value of 1.56, and L is the average intercept length, which is the line length divided by the number of grain boundaries (Mendelson 1969). The experimental conditions and results are presented in Table 1. The XRD patterns observed before heating (300 K) showed the presence of bridgmanite and

Table 1 Experimental conditions and run products

Run no	Temperature (K)	Heating rate (K/min)	Keeping time (minutes)	Cooling time (minutes)	Relative peak intensity	Apparent pressure (GPa)
Gradual heating						
FBRD06	300–547	20	–	–		
FBRD05	300–592	10	–	–		
FBRD04	300–613	10	–	10		
FBRD10	300–1079	30	–	–		
Constant temperature						
FBRD09	554	80	20	80	0.37 (2)	0.51 (6)
FBRD07	576	80	30	80	0.26 (1)	0.51 (6)
FBRD08	613	80	2*	80	0.24 (1)	0.56 (4)

*Glass capillaries broken during storage time

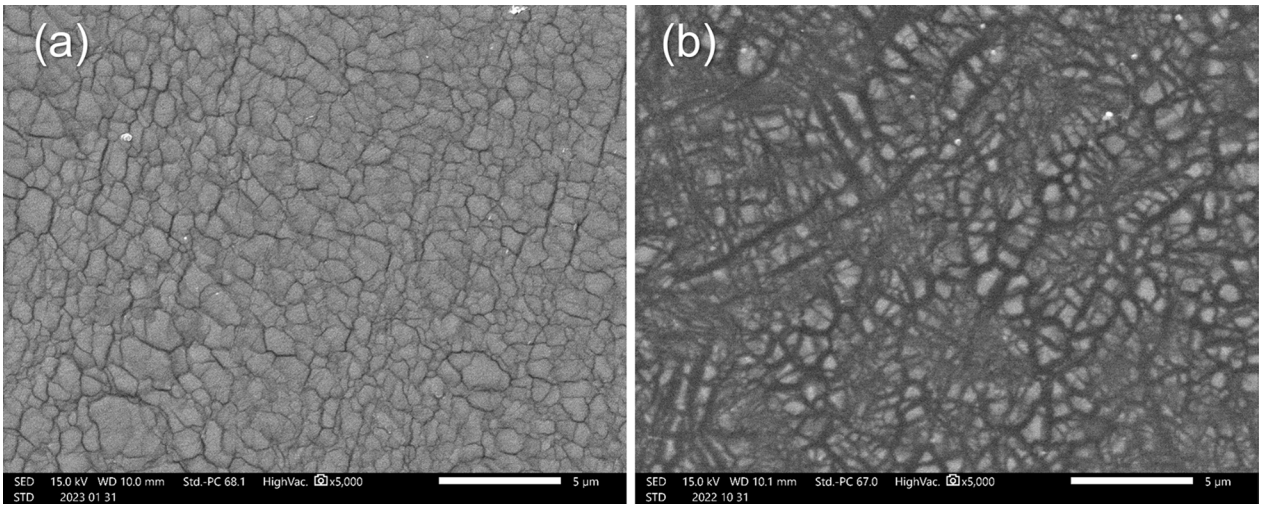

Fig. 1 Secondary electron images of bridgmanite before and after amorphization. **a** Synthesized polycrystalline bridgmanite used as starting material. **b** Partially amorphized bridgmanite after high-temperature annealing at 554 K (FBRD09). The darker regions surrounding the bridgmanite grains represent amorphous phases

trace amounts of MgO periclase (Fig. 2a). Amorphization at temperatures above 400 K induced a decrease in XRD peak intensities and also brought about the appearance of an amorphous halo (Fig. 2b), similar to the observation made in the previous study using a coarse-grained sample (Nishi et al. 2022). The XRD peaks of our synthesized fine-grained polycrystalline bridgmanite survived at temperatures up to ~ 850 K. In the previous study, it was observed that the peaks disappeared at lower temperatures (~ 700 K) (Nishi et al. 2022). Thus, the crystal structure of fine-grained bridgmanite is more robust at high temperatures.

The relative peak intensities and relative cell volumes (V/V_0) of bridgmanite as a function of temperature are shown in Fig. 3a and b, respectively. Data corresponding to coarse-grained bridgmanite polycrystalline (> 10 μm) obtained in the previous study are shown for comparison (Nishi et al. 2022). The decrease in the integrated peak intensities at temperatures above ~ 420 K indicated the partial disappearance of the bridgmanite structure owing to amorphization. The data showed that the fine-grained sample required a higher temperature for amorphization than for coarse-grained samples. Thus, the fine-grained polycrystalline bridgmanite survived at temperatures up to ~ 850 K, ~ 150 K higher than the

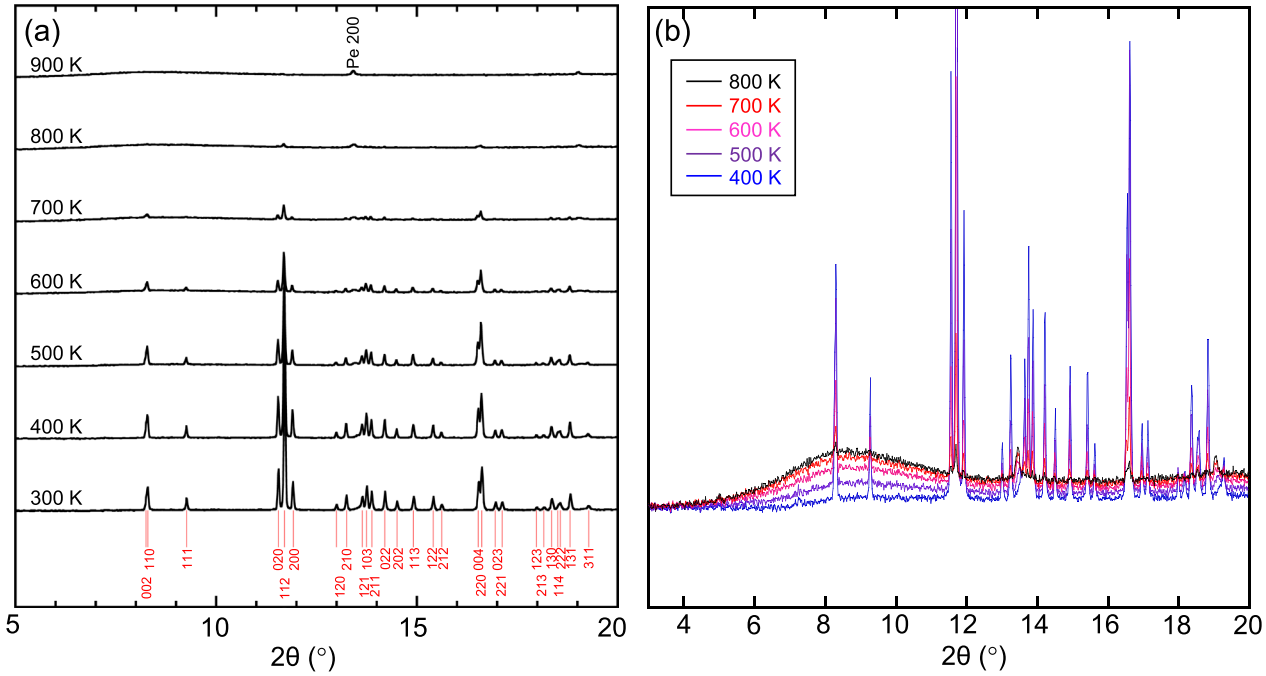

Fig. 2 **a** Selected XRD patterns during heating (FBRD10). The heating rate was 30 K/min. The vertical bars indicate peak positions calculated for bridgmanite under ambient conditions. The numbers are Miller indices. Pe, periclase. **b** Magnified XRD pattern of the near amorphous halo that appeared at a 2θ range of 3–20°. The amorphous halo signal from the glass capillary was subtracted, taking background measurements into account

maximum temperature the coarse-grained sample could survive (Fig. 3a). As previously observed, the thermal expansivity of bridgmanite decreased discontinuously following amorphization (Fig. 3b). This change could be attributed to the occurrence of stress during the amorphization process. The large difference in cell volume (~ 32%) between bridgmanite and the amorphous glass phase (Fei et al. 2021) could be attributed to the apparent pressure on bridgmanite grains experienced during amorphization. Following the previously reported method and assuming that bridgmanite has a constant thermal expansivity (2.1×10^{-5} K^{-1}) (Nishi et al. 2022), we estimated the apparent static pressure on bridgmanite during amorphization based on the compressibility of its structure as shown in Fig. 3c. The apparent pressure on bridgmanite increased due to increasing temperature, reaching ~ 1.1 GPa at 750 K. All lattice axes showed the stress effect (Fig. 4). We also observed that the peak intensities and apparent pressure were maintained during the cooling process (Fig. 5). Thus, the amorphization-induced stress could be maintained at ambient temperature.

The amorphization of bridgmanite in meteorites should proceed continuously as long as the residual post-shock residual temperature is maintained. Figure 6 shows the relative peak intensities during the heating process as a function of time. In these runs, the temperature was rapidly increased to the target value at a heating rate of 80 K/min and maintained for 2–30 min. The short heating run at 613 K was due to the breakdown of the glass capillary during heating. As previously observed, the peak intensity suddenly decreased before the target temperature was attained and did not change significantly when the temperature was kept constant. The kinetic data were analyzed using the Avrami rate equation:

$$X = 1 - \exp\left(-kt^{n}\right) \quad (1)$$

where X represents the transformed (amorphous) volume fraction, k and n are constants, and t represents the duration over which the temperature was maintained. The k and n values obtained are listed in Table 2. The n values obtained in this study (very low n values, less than ~ 0.1) were consistent with that reported by Nishi et al. (2022) for coarse-grained polycrystalline bridgmanite.

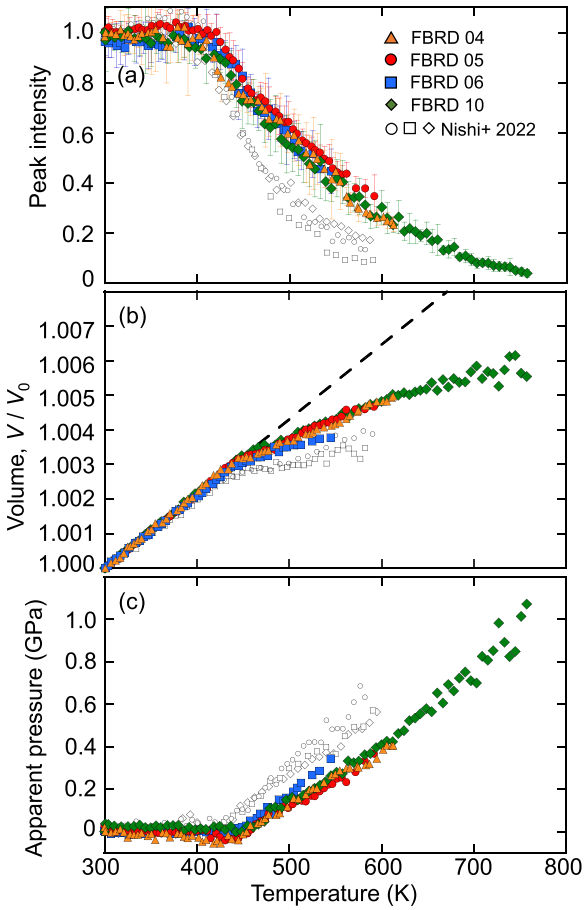

Fig. 3 High-temperature behavior of polycrystalline bridgmanite with different grain sizes. The data for the coarse-grained polycrystalline bridgmanite (> 10 μm) are based on a previous study (Nishi et al. 2022). **a** Bridgmanite peak intensities as a function of temperature. The error bars reflect the standard deviations (1σ) derived taking into consideration the various diffraction peaks. **b** Variation of relative volume (V/V_0) as a function of temperature. The dashed line shows the thermal expansivity of bridgmanite. **c** Apparent pressure on bridgmanite grains. We did not determine pressure values at temperatures above 750 K due to the weak peak intensities observed

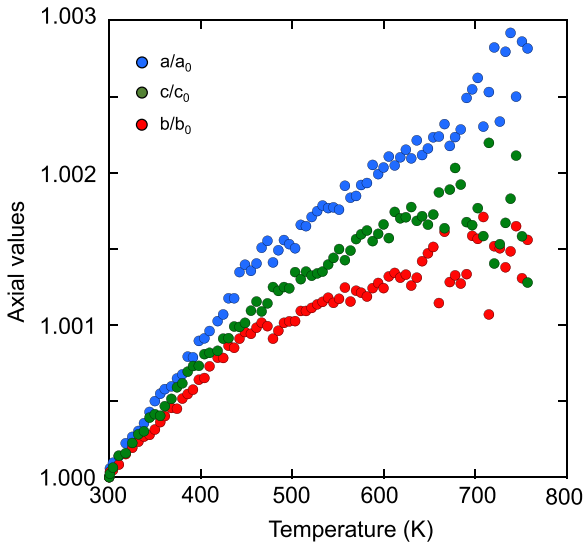

Fig. 4 Unit cell parameters of bridgmanite as a function of the temperature (FBRD10). The thermal expansivity decreased discontinuously following amorphization at above ~ 420 K

4 Discussion

Low n values in the Avrami rate equation indicated that the amorphization progress was hindered immediately after its occurrence. Further, these values differed from the general n values above 0.5, indicating continuous reaction progress over time (e.g., Kubo et al. 2004; Starink 2001). Owing to the extremely low n value, the bridgmanite volume fraction almost stagnated with time (Fig. 6b), even if the post-shock residual temperature is maintained long-term after shock events (Nishi et al. 2022).

This study, as well as a previous study (Nishi et al. 2022), has shown consistent results that bridgmanite amorphization induces static stress, which prevents further amorphization. The temperature required for amorphization differs depending on grain size, as shown in Fig. 3. However, it appeared that the relationship between apparent pressure and the bridgmanite fraction surviving after amorphization remained unchanged irrespective of grain size (Fig. 7). Therefore, it is reasonable to consider that the amorphization induced apparent pressure. Further, a recent experimental study on bridgmanite amorphization under pressure shows that the pressure increases the amorphization temperature (Kubo et al. 2022). Thus, the hindering of amorphization progress by apparent pressure is plausible. Without the effect of apparent pressure on amorphization kinetics, bridgmanite would disappear during long post-shock annealing at above ~ 420 K.

We obtained apparent pressures of up to 1.1 GPa using strong XRD peaks from bridgmanite at 750 K (Fig. 3c). The XRD patterns observed at higher temperatures showed the survival of a small amount of bridgmanite at temperatures up to ~ 850 K, although the peak intensity was not strong enough to determine the cell parameters. Using the linear correlation between apparent pressure and temperature (Fig. 3c), the pressure possibly reached ~ 1.4 GPa at 850 K.

In many cases of polycrystalline materials, polymorphic transformation proceeds via interface-controlled growth, following nucleation at the grain boundary. Therefore, the overall reaction rate should be faster

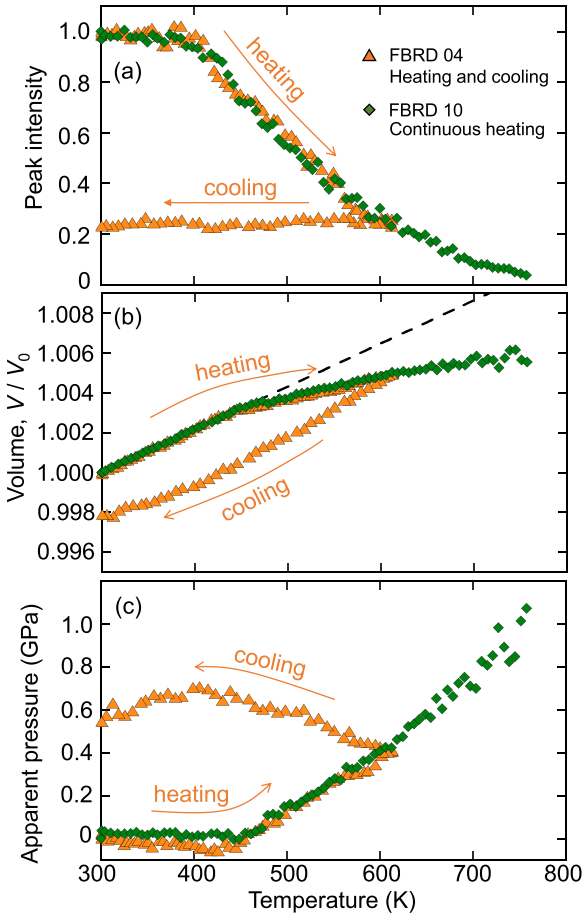

Fig. 5 High-temperature behavior of fine-grained polycrystalline bridgmanite during heating and cooling processes (FBRD04). The behavior during continuous heating (FBRD10) is shown for comparison. **a** Bridgmanite peak intensities as a function of temperature. The peak intensity was maintained during the cooling process. **b** Variation of relative unit cell volume (V/V_0) as a function of temperature. The dashed line shows the thermal expansivity of bridgmanite. **c** Apparent pressure on bridgmanite grains. The amorphization-induced stress was maintained during the cooling process

for smaller grains, which have a larger grain boundary area (Cahn 1956; Rubie and Ross 1994). In contrast, our results showed a faster amorphization rate for coarse-grained polycrystalline bridgmanite (Fig. 3). We consider that intracrystalline amorphization contributes to the amorphization process for coarse-grained polycrystalline. Actually, a previous study indicated that amorphization of coarse-grained bridgmanite occurs inside the grains rather than at grain boundaries, possibly via the use of specific locations, such as twin planes and subgrain boundaries (Nishi et al. 2022). Because intracrystalline amorphization has not been observed in fine-grained natural bridgmanite, grain boundary amorphization may be the dominant mechanism for bridgmanite amorphization in shocked meteorites.

Figure 8 shows the relationship between temperature and the amorphous molar fraction with various heating timescales. Owing to differences in grain size, the post-shock residual temperatures estimated in this study were higher than those reported in a previous study (Nishi et al. 2022). This difference may be due to intracrystalline amorphization in coarse grains, as discussed above. Considering the small grains in natural bridgmanite (< 1 μm), the fine-grained data obtained in this study were more suitable for estimating residual post-shock temperature.

Shock conditions of bridgmanite formation within the melt vein in the Tenham meteorite were estimated to be 23 to 25 GPa and 2200 to 2400 K (Tschauner et al. 2014). If such high temperatures were maintained after shock pressure release, bridgmanite amorphization would complete even if a short timescale of 10^{-2} s (Fig. 8). Thus, it is reasonable to consider that the shock vein was cooled to a temperature roughly equivalent to that of the host rock before the shock pressure was released. This result is consistent with the previous estimation based on the thermal conductivity and transformation texture of constituent minerals (Ohtani et al. 2004; Xie et al. 2006). If we assume that 10 mol% (8 vol. %) of the bridgmanite fraction survived after partial amorphization, then the estimated post-shock temperature would be ~ 700 K at a constant annealing time of 10^2 s, while this value was 600 K in the previous underestimation (Nishi et al. 2022). Thus, the amorphization mechanisms and kinetics of fine-grained bridgmanite can facilitate bridgmanite preservation in shocked meteorites. The post-shock temperature of meteorites increases with pre-impact porosity. Our estimate of the post-shock temperature is in good agreement with previous theoretical estimate for the Tenham meteorite with 7% porosity (~ 620 K) rather than that for the zero-porosity case (~ 400 K) (~ 620 K) rather than that assuming non-porous case (~ 400 K) (Xie et al. 2006).

Bridgmanite and its amorphous phase found in shocked meteorites have various chemical composition, including Fe and Al, which may affect the amorphization mechanisms and kinetics. Further experiments using Fe- and Al-bearing samples would contribute to constraining the precise residual temperature.

5 Conclusions

The amorphization mechanisms and kinetics of fine-grained polycrystalline bridgmanite were investigated via time-resolved synchrotron XRD measurements. Thus, we observed that irrespective of grain size,

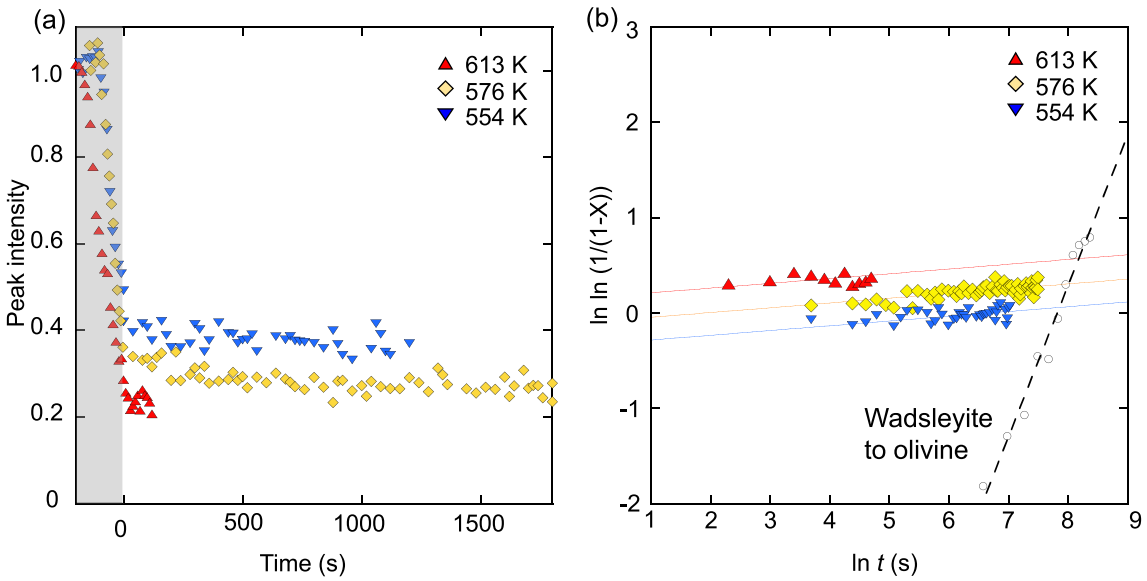

Fig. 6 **a** Plot of peak intensities as a function of time. Data were obtained from runs with the target temperatures varying in the range of 554–613 K. The heating rate was 80 K/min. The temperatures were maintained from 0 s after the initial temperature increase (shaded area). **b** Plots of ln ln(1/(1 − *X*)) as a function of ln (*t*) for the kinetic data at constant temperatures. The *n* values in the rate Eq. (1) correspond to the linear slope of these plots. The solid lines shown in this figure are based on a fixed *n* value of 0.05. The back-transition kinetics from Mg_2SiO_4 wadsleyite to olivine at 1273 K (*n* = 1.5) (Ming et al. 1991) is also provided for comparison (dashed line)

Table 2 Estimated values of kinetic parameters for bridgmanite amorphization

Run No	Temperature (K)	*n*	ln *k*	ln *k* for the *n* value of 0.05
FBRD09	554	0.03 (1)	−0.23 (7)	−0.33 (1)
FBRD07	576	0.06 (1)	−0.16 (5)	−0.10 (1)
FBRD08	613	0.00 (2)	0.34 (8)	0.16 (2)

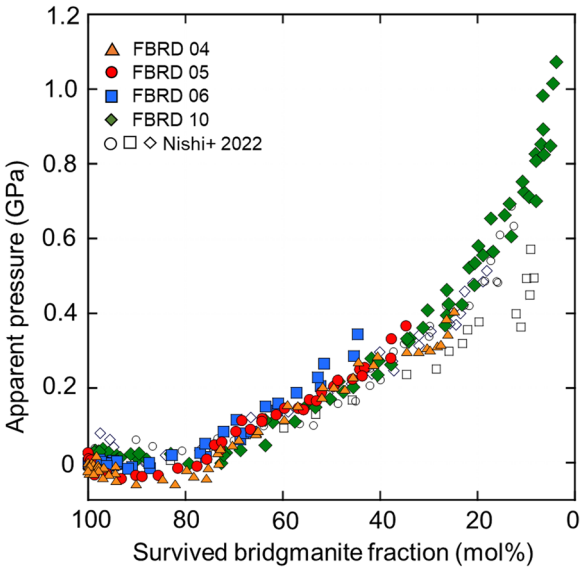

Fig. 7 Plots of the apparent pressure of bridgmanite as a function of the bridgmanite fraction that survived amorphization

significant volume expansion due to amorphization induced static stress, which prevented further amorphization. Intracrystalline amorphization initiated from twin planes and/or subgrain boundaries in bridgmanite grains may contribute to the amorphization kinetics. Thus, we observed that a higher temperature is required to induce bridgmanite amorphization for finer grains than for coarse grains. Considering the small grains in natural bridgmanite (< 1 μm), grain boundary amorphization may be the dominant amorphization mechanism for bridgmanite in shocked meteorites. The survival of 10 mol% bridgmanite requires a residual temperature of ~ 700 K, which is 100 K higher than the previously estimated temperature using data corresponding to coarse grains. The preservation of bridgmanite in meteorites can be explained by the amorphization-induced stress during post-shock annealing.

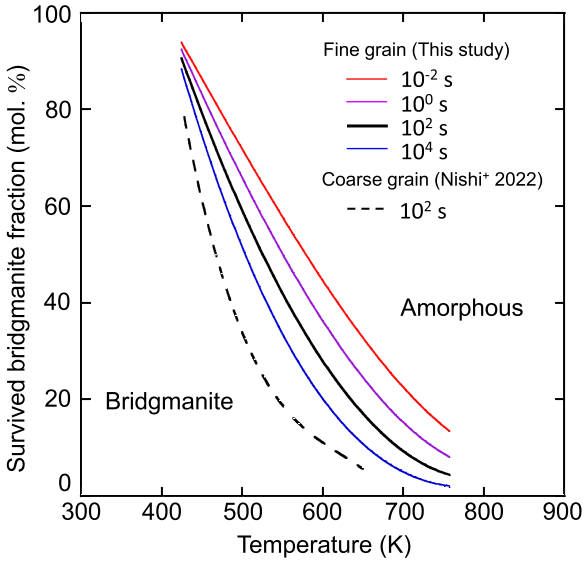

Fig. 8 Survived bridgmanite fraction after amorphization as a function of temperature. The solid curve shows the variation between the bridgmanite and amorphous fractions with different timescales of 10^{-2}–10^{4} s based on the Avrami component *n* of 0.05. The fraction change of coarse grains (Nishi et al. 2022) is also shown for comparison (dashed curve). Assuming the fine-grained polycrystalline bridgmanite, the residual post-shock temperature was estimated to be ~ 700 K when 10 mol% of bridgmanite was preserved in the shocked meteorite at a timescale of 10^{2} s. This temperature was 100 K higher than the previously estimated value assuming coarse grains

Abbreviation

XRD X-ray diffraction

Acknowledgements

We thank Takumi Miura, Masakazu Ohno, Miyuu Soejima, and Ryo Tsuruoka for their assistance with the experiments. We also thank Haruhiko Dekura for valuable comments. Fruitful comments by Dr. Naotaka Tomioka and Dr. Kishan Tiwari have greatly improved the quality of the manuscript. In situ X-ray measurements were conducted at SPring-8 (Proposal No. 2022A1110). The bridgmanite synthesis experiments were supported by the Joint Usage/Research Center of PRIUS, Ehime University, Japan.

Author contributions

MN, TK, and TS proposed the topic and designed the study. MN, SJ, KK, SK, and YM performed experiments. MN, HK, and AY synthesized the polycrystalline bridgmanite. MN wrote the manuscript. All authors have read and approved the final version of the manuscript.

Funding

This work was supported by JSPS KAKENHI (grant number JP22H01322).

Availability of data and materials

The datasets supporting the conclusions of this article are included within the article.

Declarations

Competing interests

The authors declare that they have no competing interests.

Received: 27 March 2023 Accepted: 16 July 2023
Published online: 27 July 2023

References

Beck P, Gillet Ph, El Goresy A, Mostefaoui S (2005) Timescales of shock processes in chondritic and Martian meteorites. Nature 435:1071–1074

Binns RA, Davis RJ, Reed SJB (1969) Ringwoodite, natural $(Mg, Fe)_2SiO_4$ spinel in the Tenham meteorite. Nature 221:943–944

Cahn JW (1956) The kinetics of grain boundary nucleated reactions. Acta Metall 4:449–459

Durben DJ, Wolf GH (1992) High-temperature behavior of metastable $MgSiO_3$ perovskite: a Raman spectroscopic study. Am Miner 77:890–893

El Goresy A, Dubrovinsky L, Sharp TG, Chen M (2004) Stishovite and post-stishovite polymorphs of silica in the shergotty meteorite: their nature, petrographic settings versus theoretical predictions and relevance to Earth's mantle. J Phys Chem Solids 65:1597–1608

Fei Y, Seagle CT, Townsend JP, McCoy CA, Boujibar A, Driscoll P, Shulenburger L, Furnish MD (2021) Melting and density of $MgSiO_3$ determined by shock compression of bridgmanite to 1254GPa. Nat Commun 12:876

Ghosh S, Tiwari K, Miyahara M, Rohrbach A, Vollmer C, Stagno V, Ohtani E, Ray D (2021) Natural Fe-bearing aluminous bridgmanite in the Katol L6 chondrite. Proc Natl Acad Sci U S A 118:e2108736118

Gillet P, El Goresy A (2013) Shock events in the solar system: The message from minerals in terrestrial planets and asteroids. Annu Rev Earth Planet Sci 41:257–285

Hu J, Sharp TG (2017) Back-transformation of high-pressure minerals in shocked chondrites: Low-pressure mineral evidence for strong shock. Geochim Cosmochim Acta 215:277–294

Hu J, Sharp TG (2022) Formation, preservation and extinction of high-pressure minerals in meteorites: Temperature effects in shock metamorphism and shock classification. Prog Earth Planet Sci 9:6

Kawaguchi S, Takemoto M, Osaka K, Nishibori E, Moriyoshi C, Kubota Y, Kuroiwa Y, Sugimoto K (2017) High-throughput powder diffraction measurement system consisting of multiple MYTHEN detectors at beamline BL02B2 of SPring-8. Rev Sci Instrum 88:085111

Kimura M, Chen M, Yoshida Y, El Goresy A, Ohtani E (2004) Back-transformation of high-pressure phases in a shock melt vein of an H-chondrite during atmospheric passage: implications for the survival of high-pressure phases after decompression. Earth Planet Sci Lett 217:141–150

Knittle E, Jeanloz R (1987) The activation energy of the back transformation of silicate perovskite to enstatite. Geophys Monogr Ser 39:243–250

Kubo T, Kamura K, Imamura M, Tange Y, Higo Y, Miyahara M (2022) Back-transformation processes in high-pressure minerals: Implications for planetary collisions and diamond transportation from the deep Earth. Prog Earth Planet Sci 9:21

Kubo T, Ohtani E, Funakoshi K-I (2004) Nucleation and growth kinetics of the α-β transformation in Mg_2SiO_4 determined by in situ synchrotron powder X-ray diffraction. Am Miner 89:285–293

Mendelson MI (1969) Average grain size in polycrystalline ceramics. J Am Ceram Soc 52:443–446

Ming LC, Kim YH, Manghnani MH, Usha-Devi S, Ito E, Xie HS (1991) Back transformation and oxidation of $(Mg, Fe)_2SiO_4$ spinels at high temperatures. Phys Chem Miner 18:171–179

Miyahara M, Ohtani E, Ozawa S, Kimura M, El Goresy A, Sakai T, Nagase T, Hiraga K, Hirao N, Ohishig Y (2011) Natural dissociation of olivine to $(Mg, Fe)SiO_3$ perovskite and magnesiowüstite in a shocked Martian meteorite. Proc Natl Acad Sci U S A 108:5999–6003

Nishi M, Kaneko A, Ohgidani H, Dekura H, Kakizawa S, Kawaguchi S, Kobayashi S, Sakaiya T, Kondo T (2022) Bridgmanite freezing in shocked meteorites due to amorphization-induced stress. Geophys Res Lett 49:2022GL098231

Ohtani E, Kimura Y, Kimura M, Takata T, Kondo T, Kubo T (2004) Formation of high-pressure minerals in shocked L6 chondrite Yamato 791384: Constraints on shock conditions and parent body size. Earth Planet Sci Lett 227:505–515

Ohtani E, Ozawa S, Miyahara M, Ito Y, Mikouchi T, Kimura M, Arai T, Sato K, Hiraga K (2011) Coesite and stishovite in a shocked lunar meteorite, Asuka-881757, and impact events in lunar surface. Proc Natl Acad Sci U S A 108:463–466

Rubie DC, Ross CR (1994) Kinetics of the olivine-spinel transformation in subducting lithosphere: experimental constraints and implications for deep slab processes. Phys Earth Planet Inter 86:223–243
Smith JV, Mason B (1970) Pyroxene-garnet transformation in Coorara meteorite. Science 168:832–833
Starink MJ (2001) On the meaning of the impingement parameter in kinetic equations for nucleation and growth reactions. J Mater Sci 36:4433–4441
Stöffler D, Hamann C, Metzler K (2018) Shock metamorphism of planetary silicate rocks and sediments: Proposal for an updated classification system. Meteoritn Planet Sci 53:5–49
Tiwari K, Ghosh S, Miyahara M, Ray D (2021) Shock-induced incongruent melting of Olivine in Kamargaon L6 Chondrite. Geophys Res Lett 48:e2021GL093592
Tiwari K, Ghosh S, Miyahara M, Ray D (2022) Vesicular Olivines and Pyroxenes in shocked Kamargaon L6 Chondrite: implications for primary volatiles and its multiple impacts history. J Geophys Res: Planets 127:e2022JE007420
Tomioka N, Fujino K (1997) Natural (Mg, Fe)SiO_3-ilmenite and -perovskite in the Tenham meteorite. Science 277:1084–1086
Tomioka N, Miyahara M (2017) High-pressure minerals in shocked meteorites. Meteoritn Planet Sci 52:2017–2039
Tschauner O, Ma C, Beckett JR, Prescher C, Prakapenka VB, Rossman GR (2014) Mineralogy. Discovery of bridgmanite, the most abundant mineral in Earth, in a shocked meteorite. Science 346:1100–1102
Wang Y, Guyot F, Liebermann RC (1992) Electron microscopy of (Mg, Fe)SiO_3 perovskite: evidence for structural phase transitions and implications for the lower mantle. J Geophys Res 97:12327–12347
Xie Z, Sharp TG, DeCarli PS (2006) High-pressure phases in a shock-induced melt vein of the Tenham L6 chondrite: Constraints on shock pressure and duration. Geochim Cosmochim Acta 70:504–515

Publisher's Note